CHINESE OPTICS LETTERS

Vol. 21, No. 1 | January 2023

Simultaneous temperature and magnetic field measurements using time-division multiplexing

Haobin Lin (林豪彬)[1,2,3], Ce Feng (冯 策)[1,2,3], Yang Dong (董 杨)[1,2,3], Wang Jiang (江 旺)[1,2,3], Xuedong Gao (高学栋)[1,2,3,4], Shaochun Zhang (张少春)[1,2,3*], Xiangdong Chen (陈向东)[1,2,3], and Fangwen Sun (孙方稳)[1,2,3]

[1] CAS Key Laboratory of Quantum Information, University of Science and Technology of China, Hefei 230026, China

[2] CAS Center for Excellence in Quantum Information and Quantum Physics, University of Science and Technology of China, Hefei 230026, China

[3] Hefei National Laboratory, University of Science and Technology of China, Hefei 230088, China

[4] National Key Laboratory of ASIC, Hebei Semiconductor Research Institute, Shijiazhuang 050051, China

*Corresponding author: zscyw@ustc.edu.cn

Received May 18, 2022 | Accepted August 4, 2022 | Posted Online September 13, 2022

Nitrogen-vacancy color centers can perform highly sensitive and spatially resolved quantum measurements of physical quantities such as magnetic field, temperature, and pressure. Meanwhile, sensing so many variables at the same time often introduces additional noise, causing a reduced accuracy. Here, a dual-microwave time-division multiplexing protocol is used in conjunction with a lock-in amplifier in order to decouple temperature from the magnetic field and vice versa. In this protocol, dual-frequency driving and frequency modulation are used to measure the magnetic and temperature field simultaneously in real time. The sensitivity of our system is about 3.4 nT/$\sqrt{\text{Hz}}$ and 1.3 mK/$\sqrt{\text{Hz}}$, respectively. Our detection protocol not only enables multifunctional quantum sensing, but also extends more practical applications.

Keywords: quantum sensing; temperature measurement; magnetic field measurement.
DOI: 10.3788/COL202321.011201

1. Introduction

Nitrogen-vacancy (NV) color centers are emerging solid-state quantum sensors that can measure several physical quantities using different detection protocols due to the influence of physical quantities variations such as magnetic field[1,2], electric field[3], temperature[4–7], and stress[8]. With the advantages of high spatial and temporal resolution, high sensitivity, stable signal, and quantum performance at room temperature, NV color centers can provide an effective means of characterization in a variety of fields, including biomedicine[9], dark matter[10], electrochemical signals[11], etc. The sensitivity can be further enhanced by utilizing phase-sensitive detection, which reduces ambient F-noise, allowing for more stable detection of signals and higher sensitivity[12–20].

The extraordinary sensitivity of NV and multiple physical quantity sensing raise the experimental environment requirements and limit the application scenarios, making quantum sensing less practical. Magnetic and temperature noises are present in most sensor environments. Utilizing double-quantum (DQ) coherence technology or multitone microwaves (MWs) can reduce noise interference efficiently[21]. These protocols, however, can only measure a single physical quantity and does not take full advantage of the multi-physics sensing characteristics of NV. To achieve stable and highly sensitive measurements of the magnetic field and temperature, some research groups have used time-division and frequency-division multiplexing methods[22,23]. Nevertheless, the existing simultaneous measurements require further processing of the signal to obtain the target data.

In this Letter, we demodulate the electrical signal of the photoelectric detector, so the temperature and magnetic field information are directly separated. Lock-in amplifiers (LIAs) deal only with temperature or magnetic field signals, so there is no need to use phase information for further processing, which makes the measurement method more robust.

2. Methods

At room temperature, NV centers demonstrate a long spin lifetime and an electronic ground state of spin 1 triplet state, and they can function as a multimodal sensor due to their spin energy levels that are sensitive to magnetic, electric, strain, and temperature variations. The ground state of NV is a spin triplet, whose degeneracy is lifted by spin-spin interactions into a singlet state of spin projection $|0\rangle$ and a doublet state $|\pm 1\rangle$ in the absence of a magnetic field. Resonant MWs are applied near 2.87 GHz to achieve coherent spin control. Through optical excitation, spin initialization to $|0\rangle$, and nonradiative decay

through intersystem crossover, the spectrum of spin-state-dependent fluorescence, referred to as optically detected magnetic resonance (ODMR) spectroscopy, can be obtained. The frequencies of the resonance signals, denoted by $|+1\rangle$ and $|-1\rangle$, are shifted as a consequence of the Zeeman effect when an external magnetic field is applied, as schematically shown in Fig. 1(a). Using ODMR spectroscopy, we can determine the energy levels and, therefore, the magnitude of the physical quantities. If the energy level shift associated with a change of physical quantity is smaller than the ODMR linewidth, the signal change of the fixed single-point detection fluorescence can provide a quick indication of the value. For our experiments, we selected five points of f_0 to f_4 for the measurement of temperature and magnetic field. By sweeping the MW frequency, the ODMR spectrum of resonant transitions of $|0\rangle \rightarrow |-1\rangle$ and $|0\rangle \rightarrow |+1\rangle$ is plotted in Fig. 1(b), where the horizontal coordinate is the applied MW frequency, and the vertical coordinate is the demodulated voltage signal R. Linewidth is approximately 8 MHz. Positions 1–4 correspond to the maximum slope of ODMR. Based on the detection protocol and the time-division demodulation method, the R obtained from demodulating the signal connected to the LIAs contains information about the magnetic field or about the temperature.

Diamond with dimensions of 200 μm × 200 μm × 100 μm has been grown in chemical vapor deposition with [111] crystal-oriented crystals. Figure 1(c) shows that the diamond is combined with a composite parabolic lens (CPC) with UV solid-state adhesive. The 532 laser (MGL-N-532A) illuminates from inside the 200 μm fiber, while the fluorescence signal was collected from the other side of the diamond. Copper wire is used as an antenna. The fluorescence light is collected into the monitor negative port of the balanced photodetector (PDB210A) after passing through the bandpass filter (FF01-709/167-25).

For the photodetector, the positive port on the monitor is connected to a 200 μm optical fiber. In time-division demodulation, the two outputs of the detector signal (monitor+, monitor-) of the photodetector are, respectively, connected to two MW switches (ZASWA-2-50DRA+, SW). The timing signal demodulation from the MW switch is controlled by a pulse generator (PBESR-PRO-500-PCIe), and the outputs of the MW switch are linked to different LIAs.

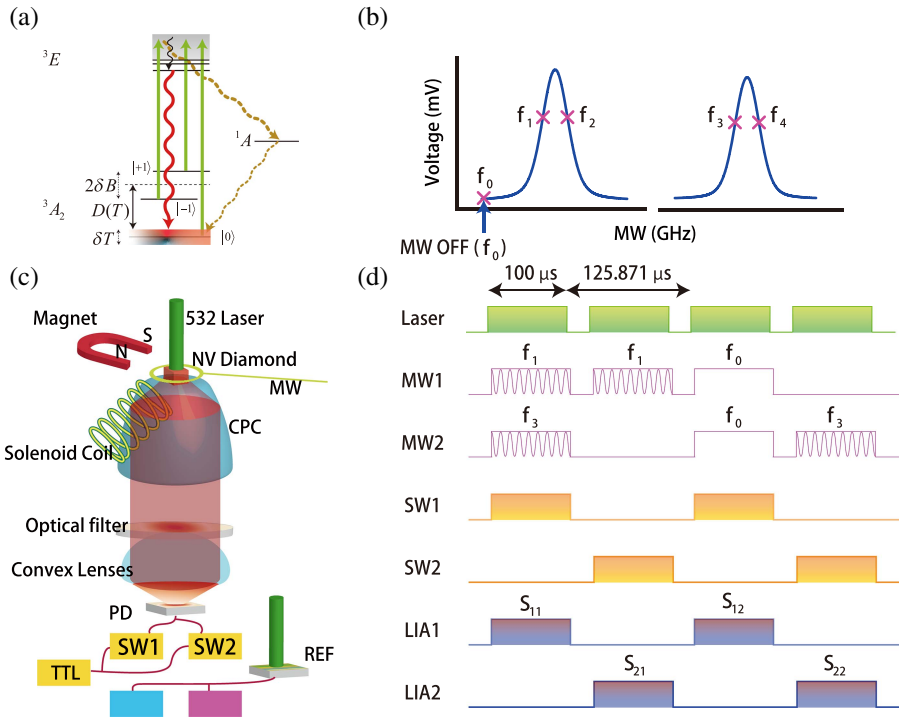

Fig. 1. (a) NV center energy level diagram, with zero-field splitting D between ground-state electronic spin levels $|0\rangle$ and $|\pm1\rangle$. In the presence of a magnetic field, energy levels $|\pm1\rangle$ experience a Zeeman shift, which forms the basis of NV magnetometry. The NV thermometer is based on the $|0\rangle$ energy level shifting with temperature. (b) ODMR spectrum of the diamond sensor under a DC bias magnetic field of 46 Gauss, provided by a permanent magnet beneath the head. f_0 is far off resonant frequency. f_1 to f_4 are the maximum slopes of the ODMR spectral line, respectively. (c) Configuration of a time-division multiplexing diamond sensor. A CPC on the bottom of the NV diamond sample, combined with an optical filter and convex lens, guides fluorescence from NV centers to the photodiode. The additional 532 laser is used for reference signals. The pulse generator modulates SW1 and SW2 by means of TTL signals. The output signal of SW1 and SW2 only contains temperature and magnetic field information, and it is sent to LIA1 and LIA2 for processing. (d) Diagram of a time-domain multiplexed frequency modulation time sequence. S_{11}–S_{12} shows that the signal seen by LIA1 has temperature information. S_{21}–S_{22} shows that the signal measured by LIA2 gives information about the magnetic field.

To achieve time-division multiplexing and reduce MW resources, we combine dual-frequency driving with frequency modulation, which allows simultaneous measurement of temperature and magnetic field with half the number of MW sources. Two MWs are used simultaneously at the place of maximum slope (denoted as $f_1 + f_3$), and frequency modulation applies two MWs at different times (denoted as $f_1 - f_3$). Since the signal to be measured must be oscillating at a certain frequency, the dual-frequency drive must be coupled to a virtual frequency f_0 (f_0 is non-resonant), and hence both approaches have the same period.

It has been shown that temperature and magnetic fields can be measured simultaneously by using both time division and frequency division[22,23]. The previous experiments required precise phase modulation, which made the experiment more complex, and both approaches obtained the temperature and magnetic field signals indirectly by obtaining orthogonal X and Y signals and then processing the data. By combining dual-frequency driving and time-division demodulation, we can minimize the number of MW sources, which is consistent with frequency-division multiplexing. With this method, the demodulated signals are connected to two LIAs, and the temperature or magnetic field information is directly derived from the demodulated R of the amplifiers:

$$T^{\mathrm{meas}} \propto S_{11} - S_{12}, \tag{1}$$

$$B^{\mathrm{meas}} \propto S_{21} - S_{22}, \tag{2}$$

where T^{meas} and B^{meas} are the measured magnetic field and temperature, respectively. S_{11} to S_{22} are the four data acquisitions presented in Fig. 1(d). So, this is a direct simultaneous measurement for conventional LIAs.

3. Experimental Results and Discussion

Because continuous ODMR spectra are subject to laser and MW power, which results in broadening effects and thus reduced sensitivity, in our experiment, ODMR was measured as a function of temperature and magnetic field. The signal modulation frequency was set to about 2.21 kHz, and the time constant was about 15 ms. A quasi-continuous approach is used to reduce the heating effect of the laser. Figure 2 shows the ratio of the peak value and the peak width of the measured ODMR signal. As the point with the largest ratio indicates the greatest sensitivity[24], this point is used in the next step of the measurement.

Hereafter, we test the robustness of the temperature measurement and magnetic field measurement. In the configuration of temperature sensing, since the laser itself produces a heating effect on the diamond, the performance of different probing protocols can be investigated by measuring such a heating process. First, the conventional fixed single-point detection method was used by setting the frequency to a specific value in order to observe the response of the fluorescence voltage to temperature and magnetic field. As shown in Fig. 3(a), the experiment was

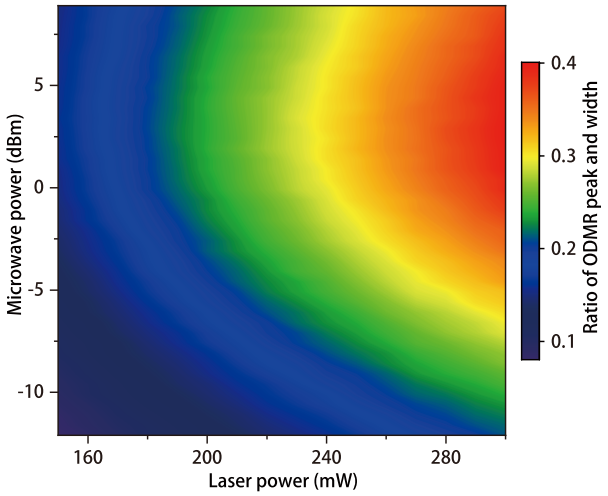

Fig. 2. Contour plot of the ratio of ODMR peak and width as a function of light power and MW power.

measured for 5 s and repeated 10 times, and, at the position of around 0.5 s, the interference of the magnetic field became apparent.

A combination of detection techniques using double frequency, denoted as $f_1 - f_3$ and $f_1 + f_3$ shown in Fig. 3(b), is used to suppress temperature or magnetic field fluctuations. An MW signal of $f_1 + f_3$ means that MWs are applied simultaneously, whereas a signal of $f_1 - f_3$ means MWs are applied one at a time. In this case, magnetic fields or temperature fluctuations can be derived by this method. Note that the bias magnetic field is applied at 0.5 s and shuttered at 4 s, while the temperature of diamond keeps rising due to laser heating effects. Since the temperature causes the spectral lines moving in common mode, the method of $f_1 + f_3$ obtains the temperature with the magnetic field suppressed. On the other hand, magnetic fields result in the spectral lines shifting in the differential mode. Therefore, by suppressing the temperature, $f_1 - f_3$ measures the effect of the magnetic field while suppressing the effect of the temperature. In the same way, $f_1 + f_4$ measures the magnetic field, whilst $f_1 - f_4$ measures the temperature [Fig. 3(c)].

After demonstrating the effectiveness of the magnetic field and temperature measurements, we perform an experiment of time-division demodulation on the detector. The MW switch is turned on and off by the transistor–transistor logic (TTL) signal from the pulse generator, and the RF output of the MW switch is connected to each of the two LIAs by applying the same time period selection. In LIA1, the signal only contains information about the temperature, while, in LIA2, the signal only contains information about the magnetic field. After demodulation, the R values are shown in Fig. 3(d). The simultaneous measurements show that the mutual coupling between temperature and magnetic field can be eliminated.

As R is used for sensing and independent of the modulation phase, there is no need to consider phase synchronization. For our sensing protocol, the phases of X and Y are discontinuous in the single-shot experiment. In time-division multiplexing

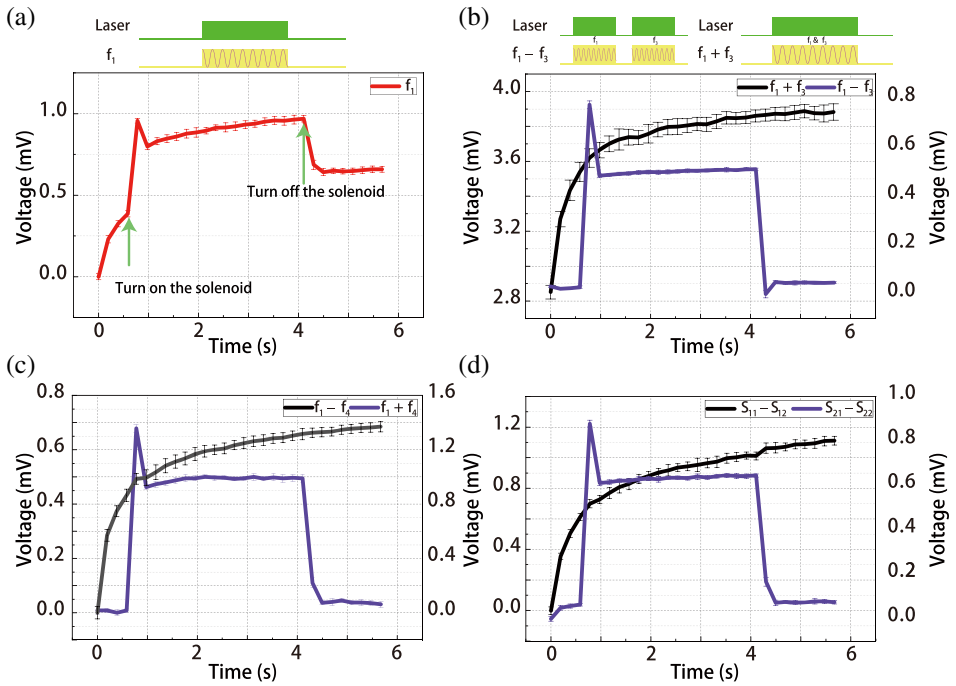

Fig. 3. Confirmation of simultaneous temperature and magnetic field measurements. (a) Demodulated amplitude value of R of the LIA. The measurement was performed in an environment where a bias magnetic field was applied, the jitter in 0.5 s was caused by activating the electromagnet, and the temperature change was caused by the laser heating after starting the measurement. (b), (c) Dual-frequency driving and frequency modulation are used to measure magnetic fields and temperatures. f_1–f_3 ($f_1 - f_4$) indicates that the MWs are applied separately in time. $f_1 + f_3$ ($f_1 + f_3$) indicates that MWs are applied simultaneously in time. (d) Temperature and magnetic field measurements taken simultaneously; $S_{11} - S_{12}$ are the results of LIA1 measurements, which only give temperature. $S_{21} - S_{22}$ are the results of LIA2 measurements, which only give magnetic field.

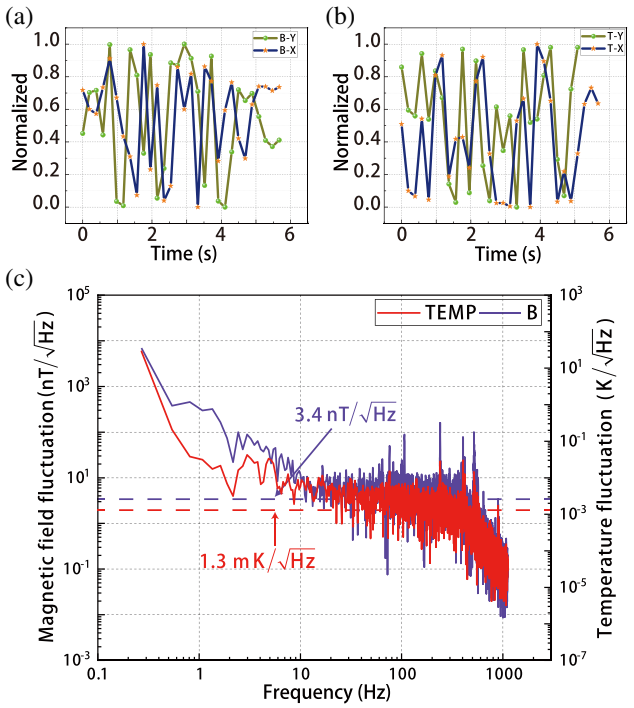

Fig. 4. (a), (b) *X* and *Y* are measured under the condition of time-divided measurements. B-X and B-Y are modulated by LIA1. T-X and T-Y are demodulations by LIA2. A magnetic field of 0.2 mT is applied at 0.5 s. (c) Sensitivity is measured as noise power and frequency spectrum.

measurements, B-X and B-Y represent the *X* and *Y* signals of magnetic field measurements, and T-X and T-Y represent temperature measurements, as shown in Figs. 4(a) and 4(b). It can be clearly seen that the phase of *X* and the phase of *Y* are disorderly. Since the amplitude value of R is independent of the phase of *X* and *Y*, the measurement error due to phase mismatch is ignored. Therefore, our measurement method is more robust compared to the tracking phase method[15,25]. In the end, the noise spectrum obtained from the time-division signal was measured. Hamming windows were used to obtain the magnetic field and temperature noise spectra, as plotted in Fig. 4(c). The sensitivity of our system is about $3.4\,\mathrm{nT}/\sqrt{\mathrm{Hz}}$ and $1.3\,\mathrm{mK}/\sqrt{\mathrm{Hz}}$, respectively.

4. Conclusion

In summary, we present a detection protocol for temperature and magnetic field measurement without phase synchronization. When performing high-sensitivity magnetic field or temperature measurements, the experimental environment is often full of unwanted electromagnetic or temperature disturbances. In the case of magnetic field measurements, even though the quasi-continuous excitation method reduces the heating effect of the laser, the excited laser is sufficient to produce temperature interference. We have used electrical signal time-division multiplexing demodulation to separate the optically mixed

signals containing temperature and magnetic field information, so that simultaneous temperature and magnetic field measurements can be achieved. Since the temperature and magnetic field information is obtained directly from the signal amplitude values, this sensing method is more robust, which enables more practical applications of quantum measurements.

Acknowledgement

This work was supported by the National Natural Science Foundation of China (Nos. 12005218 and 52130510).

References

1. J. R. Maze, P. L. Stanwix, J. S. Hodges, S. Hong, J. M. Taylor, P. Cappellaro, L. Jiang, M. V. G. Dutt, E. Togan, A. S. Zibrov, A. Yacoby, R. L. Walsworth, and M. D. Lukin, "Nanoscale magnetic sensing with an individual electronic spin in diamond," Nature **455**, 644 (2008).
2. X.-D. Chen, E.-H. Wang, L.-K. Shan, C. Feng, Y. Zheng, Y. Dong, G.-C. Guo, and F.-W. Sun, "Focusing the electromagnetic field to $10^{-6}\lambda$ for ultra-high enhancement of field-matter interaction," Nat. Commun. **12**, 6389 (2021).
3. F. Dolde, H. Fedder, M. W. Doherty, T. Nöbauer, F. Rempp, G. Balasubramanian, T. Wolf, F. Reinhard, L. C. L. Hollenberg, F. Jelezko, and J. Wrachtrup, "Electric-field sensing using single diamond spins," Nat. Phys. **7**, 459 (2011).
4. V. M. Acosta, E. Bauch, M. P. Ledbetter, A. Waxman, L. S. Bouchard, and D. Budker, "Temperature dependence of the nitrogen-vacancy magnetic resonance in diamond," Phys. Rev. Lett. **104**, 070801 (2010).
5. X.-D. Chen, C.-H. Dong, F.-W. Sun, C.-L. Zou, J.-M. Cui, Z.-F. Han, and G.-C. Guo, "Temperature dependent energy level shifts of nitrogen-vacancy centers in diamond," Appl. Phys. Lett. **99**, 161903 (2011).
6. S.-C. Zhang, S. Li, B. Du, Y. Dong, Y. Zheng, H.-B. Lin, B.-W. Zhao, W. Zhu, G.-Z. Wang, X.-D. Chen, G.-C. Guo, and F.-W. Sun, "Thermal-demagnetization-enhanced hybrid fiber-based thermometer coupled with nitrogen-vacancy centers," Opt. Mater. Express **9**, 4634 (2019).
7. S.-C. Zhang, Y. Dong, B. Du, H.-B. Lin, S. Li, W. Zhu, G.-Z. Wang, X.-D. Chen, G.-C. Guo, and F.-W. Sun, "A robust fiber-based quantum thermometer coupled with nitrogen-vacancy centers," Rev. Sci. Instrum. **92**, 044904 (2021).
8. P. Ovartchaiyapong, K. W. Lee, B. A. Myers, and A. C. B. Jayich, "Dynamic strain-mediated coupling of a single diamond spin to a mechanical resonator," Nat. Commun. **5**, 4429 (2014).
9. C. Li, R. Soleyman, M. Kohandel, and P. Cappellaro, "SARS-CoV-2 quantum sensor based on nitrogen-vacancy centers in diamond," Nano. Lett. **22**, 43 (2022).
10. M. C. Marshall, M. J. Turner, M. J. H. Ku, D. F. Phillips, and R. L. Walsworth, "Directional detection of dark matter with diamond," Quantum Sci. Technol. **6**, 024011 (2021).
11. H. T. Dinani, E. Muñoz, and J. R. Maze, "Sensing electrochemical signals using a nitrogen-vacancy center in diamond," Nanomaterials **11**, 358 (2021).
12. L. Rondin, J.-P. Tetienne, P. Spinicelli, C. D. Savio, K. Karrai, G. Dantelle, A. Thiaville, S. Rohart, J.-F. Roch, and V. Jacques, "Nanoscale magnetic field mapping with a single spin scanning probe magnetometer," Appl. Phys. Lett. **100**, 153118 (2012).
13. H. A. R. El-Ella, S. Ahmadi, A. M. Wojciechowski, A. Huck, and U. L. Andersen, "Optimised frequency modulation for continuous-wave optical magnetic resonance sensing using nitrogen-vacancy ensembles," Opt. Express **25**, 14809 (2017).
14. E. Moreva, E. Bernardi, P. Traina, A. Sosso, S. D. Tchernij, J. Forneris, F. Picollo, G. Brida, Ž. Pastuović, I. P. Degiovanni, P. Olivero, and M. Genovese, "Practical applications of quantum sensing: a simple method to enhance the sensitivity of nitrogen-vacancy-based temperature sensors," Phys. Rev. Appl. **13**, 054057 (2020).
15. A. M. Wojciechowski, M. Karadas, C. Osterkamp, S. Jankuhn, J. Meijer, F. Jelezko, A. Huck, and U. L. Andersen, "Precision temperature sensing in the presence of magnetic field noise and vice-versa using nitrogen-vacancy centers in diamond," Appl. Phys. Lett. **113**, 013502 (2018).
16. R. S. Schoenfeld and W. Harneit, "Real time magnetic field sensing and imaging using a single spin in diamond," Phys. Rev. Lett. **106**, 030802 (2011).
17. H. Clevenson, L. M. Pham, C. Teale, K. Johnson, D. Englund, and D. Braje, "Robust high-dynamic-range vector magnetometry with nitrogen-vacancy centers in diamond," Appl. Phys. Lett. **112**, 252406 (2018).
18. C. S. Shin, C. E. Avalos, M. C. Butler, D. R. Trease, S. J. Seltzer, J. P. Mustonen, D. J. Kennedy, V. M. Acosta, D. Budker, A. Pines, and V. S. Bajaj, "Room-temperature operation of a radiofrequency diamond magnetometer near the shot-noise limit," J. Appl. Phys. **112**, 124519 (2012).
19. J. M. Schloss, J. F. Barry, M. J. Turner, and R. L. Walsworth, "Simultaneous broadband vector magnetometry using solid-state spins," Phys. Rev. Appl. **10**, 034044 (2018).
20. H. Clevenson, M. E. Trusheim, C. Teale, T. Schröder, D. Braje, and D. Englund, "Broadband magnetometry and temperature sensing with a light-trapping diamond waveguide," Nat. Phys. **11**, 393 (2015).
21. E. Bauch, C. A. Hart, J. M. Schloss, M. J. Turner, J. F. Barry, P. Kehayias, S. Singh, and R. L. Walsworth, "Ultralong dephasing times in solid-state spin ensembles via quantum control," Phys. Rev. X **8**, 031025 (2018).
22. J. H. Shim, S.-J. Lee, S. Ghimire, J. I. Hwang, K.-G. Lee, K. Kim, M. J. Turner, C. A. Hart, R. L. Walsworth, and S. Oh, "Multiplexed sensing of magnetic field and temperature in real time using a nitrogen-vacancy ensemble in diamond," Phys. Rev. Appl. **17**, 014009 (2022).
23. Y. Hatano, J. Shin, D. Nishitani, H. Iwatsuka, Y. Masuyama, H. Sugiyama, M. Ishii, S. Onoda, T. Ohshima, K. Arai, T. Iwasaki, and M. Hatano, "Simultaneous thermometry and magnetometry using a fiber-coupled quantum diamond sensor," Appl. Phys. Lett. **118**, 034001 (2021).
24. J. F. Barry, J. M. Schloss, E. Bauch, M. J. Turner, C. A. Hart, L. M. Pham, and R. L. Walsworth, "Sensitivity optimization for NV-diamond magnetometry," Rev. Mod. Phys. **92**, 015004 (2020).
25. I. Fescenko, A. Jarmola, I. Savukov, P. Kehayias, J. Smits, J. Damron, N. Ristoff, N. Mosavian, and V. M. Acosta, "Diamond magnetometer enhanced by ferrite flux concentrators," Phys. Rev. Res. **2**, 023394 (2020).